Tribology International 145 (2020) 106167

Contents lists available at ScienceDirect

Tribology International

journal homepage: http://www.elsevier.com/locate/triboint

A discussion on the capability of X-ray computed tomography for contact mechanics investigations

Feikai Zhang, Jianhua Liu, Xiaoyu Ding *, Zhimeng Yang

Beijing Institute of Technology, School of Mechanical Engineering, Beijing, 100081, China

ARTICLE INFO

Keywords:
Contact mechanics experiment
Area of true contact
Three-dimensional gap distribution
X-ray CT

ABSTRACT

The three-dimensional gap distribution and area of true contact significantly affect sealing performance and tribological properties between rough surfaces. Current experimental approaches are limited in their ability to predict the evolution of the gap distribution and real contact area on assembled rough interfaces, particularly on non-transparent surfaces. In our previous study [1], we presented a X-ray computed tomography method to obtain these parameters between non-transparent assembled rough interfaces experimentally. In this study, contacts of higher complexity than in our previous work are studied and accuracy as well as limitations of the experimental method are discussed. Additionally, the experimental procedure and data-processing methods are detailed to help other researchers reproduce this work.

1. Introduction

Surfaces at a contact interface appear flat or smooth at the macroscale, but are actually rough at the microscale. When we measure them using, for example, an optical surface profilometer, many peaks and valleys can be detected. When two rough surfaces are squeezed together, although some higher peaks may be in contact, most of the lower peaks remain separated from the opposite surface. The contact zone, which makes up only a small part of the entire contact surface, largely depends on the squeeze load, surface materials, and surface topography. The area of true contact and gap distribution (also known as surface separation), significantly affect the sealing performance [2,3] and tribological properties [4]. Thus, it is very important to have a reliable experiment method to investigate the area of true contact and gap distribution for contact mechanics.

Extensive experimental studies have been carried out to measure the real contact area between rough surfaces, some good reviews on this topic can be found in the literature [5,6]. For example, the thermal resistance [7], electric resistance [8], and ultrasonic reflection coefficient [9,10] have been measured and third bodies, such as pressure-sensitive films [11,12], polymer films [13], and gold films [6], have been used to experimentally measure the area of true contact, but all of these methods are limited in their ability to provide the distribution of the three-dimensional (3D) surface separation. Additionally, accuracy is significantly affected by the surface oxide layer [7–10] or the presence of the third bodies [6,11–13]. Optical experiments using surface profilometers [14–19] or self-designed equipment [20–23] were another kind of methods to obtain the real contact area or gap between a rough interface and a flat transparent interface. However, local stress might destroy the flatness of the transparent surface if the rough surface is not sufficiently soft compared with the transparent surface, which may affect the accuracy of the results. Furthermore, assembling rough interface with transparent rigid flat interface is not common in engineering applications. As for the experimental measurement of gap distribution or surface deformation in contact process, there are very few works. Among all the works mentioned above, only a few optical experiments [22,23] were reported to measure the surface deformation. Other experiments such as wear measurements [24,25] were also carried out to measure plastic deformation after unloading, but the measurement of the elastic deformation was unavailable. In summary, it is still a big challenge to experimentally measure the real contact area and gap distribution between rough surfaces.

CT technology is a new developed contact measurement method [26–28], which has the potential to measure both real contact area and gap distribution. Recently, we also reported an experimental method [1] to study contact mechanics between non-transparent rough surfaces by accurately measuring the area of true contact and 3D gap distribution by using X-ray CT technology; experiment results were compared with those of a finite element method (FEM) simulation. However, the detailed experimental procedure and data-processing method need to be

* Corresponding author.
E-mail address: xiaoyu.ding@bit.edu.cn (X. Ding).

https://doi.org/10.1016/j.triboint.2020.106167
Received 19 August 2019; Received in revised form 3 December 2019; Accepted 10 January 2020
Available online 11 January 2020

presented to assist other researchers to reproduce this work. Additionally, the accuracy and limitations of the experimental method required further study. Herein, the experimental procedure and data processing are described in detail for the contact between four sets of aluminum (Al) contact pairs and two sets of polycarbonates (PC) contact pairs. The accuracy and limitations of this method are also discussed. Since X-ray CT technology has scarcely been applied to contact mechanics [1,26], we believe this work will provide scientists and engineers working in this field with new ideas and contribute to novel fundamental discoveries.

2. Experimental description

2.1. CT equipment and experiment setup

High-resolution CT has become a powerful tool for a diversity of industrial, scientific, and metrological applications [29,30]. The spatial resolution (both lateral or normal resolution) of CT can be less than 200 nm [31], which meets the requirements for microcontact observations. The instrument used in this work was the phoenix nanotom® m, a 180 kV/20 W X-ray nano-CT system. Fig. 1 is an illustration of this system, which consists of a radioactive source, an objective table, and a detector. The highest possible spatial resolution of this CT equipment is 200 nm. However, the actual spatial resolution of the CT measurements is limited by the density and size of the analyte, and the experimental setup. If the density of the analyte or setup is too high, the power of X-ray might not be sufficient enough to achieve a high-resolution measurement. The size of the analyte and setup influence the spatial resolution by increasing the distance between the radioactive source and the analyte; the spatial resolution (length unit, e.g., nm) in an experiment is theoretically approximately proportional to the distance. With of all these factors considered, the actual spatial resolution achieved in this work was 2 μm.

During contact mechanics experiments, pressure must be applied and maintained to the contact interfaces. An experimental apparatus was designed to achieve this (Fig. 2). The setup consisted of a regulating bolt, transparent tube, pencil rod, pressure sensor, and load bolt, among other components. The samples were confined to the transparent tube and assembled between the regulating bolt and pencil rod, and the regulating bolt was used to align the sample to the measurement region. The squeeze load was applied by screwing the load bolt. After measurement by the sensor, the load was transmitted to the samples and finally squeezed on the rough surfaces. The tube was designed to be slender to reduce the size of the setup; this helped achieve higher-resolution CT measurements.

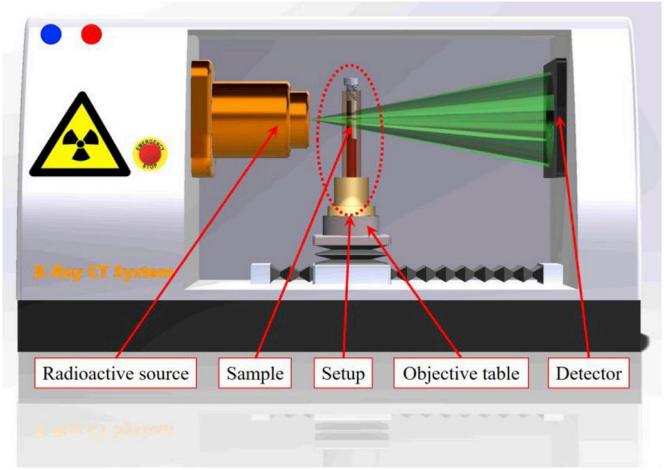

Fig. 1. The computed tomography (CT) system.

2.2. Sample preparation

Six contact pairs were examined in this work. These contact pairs were numbered from Experiment 1 to Experiment 6, and each of them was constitutive of two cylindrical experimental samples, which were numbered as Sample *x*-1 and Sample *x*-2 (*x* refers to the contact pair). Fig. 3 shows the cylindrical samples used in the experiments and their size. The end faces of the two cylinders formed a contact pair. The details of the samples are summarized in Table 1. Among these contact pairs, the material of contact pair 3 and 5 was PC, while Al was used for the other contact pairs. Contact pair 4 was composed of two isotropic random rough surfaces (Fig. 4a), while the other contact pairs were composed of a relatively rough anisotropic surface having several parallel textures (Fig. 4b) and a relatively flat surface.

2.3. Experimental procedure

Each sample was aligned to the measurement region of the apparatus. After applying the squeeze load (5, 50, 100, 200, 350, and 500 N for contact pairs 1–4; 5 and 125 N for contact pairs 5 and 6) by screwing the load bolt, the apparatus was set up on the objective table of the CT equipment. Then, the X-rays emitted by the radioactive source were passed through the sample and detected and recorded by the detector. The objective table was then rotated to a new position by a preset number of degrees, and the sample was irradiated by additional X-rays. The detection procedure continued until the objective table had been rotated by 360°. The data recorded in each position were processed based on tomographic reconstruction and other methods [32] to build a geometric model (Fig. 5). Specifically, this model was output in stereolithography (STL) format and contained triangulated surfaces that defined the external surfaces of the contact solids, as well as point clouds defining the corners of the triangulated surfaces.

3. Data processing and error estimation

3.1. Calculation of the surface separation and normalized real contact area

Stereolithography models are computer-aided design models that are widely used to describe the external surfaces of objects. In a contact pair, gaps exist between rough surfaces in the non-contact region, while the two solids come into contact in the contact region via the squeeze pressure. X-ray CT technology uses density contrast to identify the boundary of an analyte. The materials of Samples *x*-1 and *x*-2 were the same in this work; consequently, only the rough surfaces in the non-contact region were identified as the external surfaces. Fig. 6 is a sketch of the STL model of an experimentally observed contact pair. The red solid circles and lines correspond to the point cloud and triangulated surfaces on the upper rough surface, respectively, while the blue dashed circles and lines correspond to the point cloud and triangulated surfaces on the lower rough surface, respectively. The cavities between Samples *x*-1 and *x*-2 in section view A are non-contact regions, and the other zones between the samples occupied by the solid material are contact regions. There are no point clouds or triangulated surfaces in the STL models to define the boundary between Sample *x*-1 and *x*-2 in the contact regions, and the point clouds in the non-contact regions are not ordered. Experimental data need to be further processed to obtain the area of true contact and surface separation, and to help with further analysis of the contact behavior.

A two-dimensional array is commonly used to describe the topography of a rough surface or the gap distribution between a contact pair. Each array element represents a point on the *xy* plane, and the spacing between these points is equal. In this study, the data of the STL model were processed to yield an array representing the surface separation, and to calculate the real contact area. The data processing is actually an interpolation process. Both linear interpolation and cubic interpolation

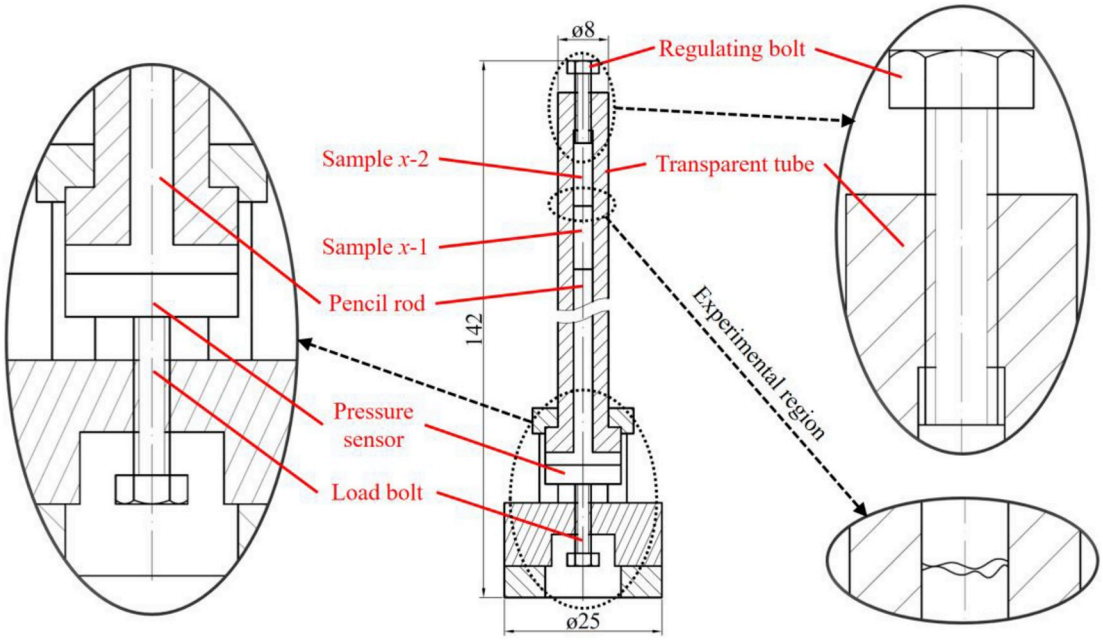

Fig. 2. Experimental setup.

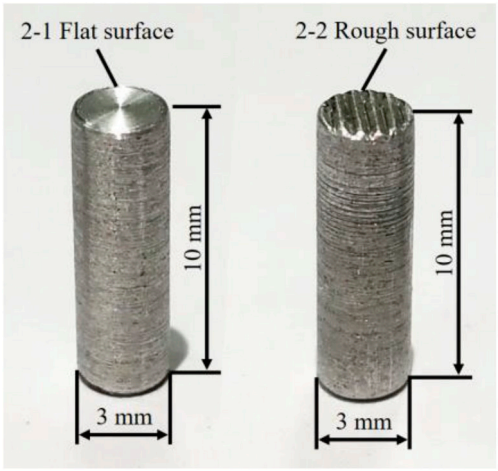

Fig. 3. Experimental samples 2–1 and 2-2.

have been employed, and it was found that the effect of interpolation method on real contact area, gap distribution, surface roughness (RMS) and root mean square slope was negligible. As linear interpolation is less complicated, it was used in this work. During the data processing, the rough surfaces were assumed to be parallel to the *xy* plane and a grid, which consisted of a set of nodes p_{ij} ($i = 1, 2\ldots, I; j = 1, 2, \ldots, J$), was defined on the *xy* plane. The coordinate of node p_{ij} is $(x_i, y_j, 0)$, where $x_i = (i-1)\cdot d$, $y_i = (j-1)\cdot d$, and d is the spacing between nodes. Then, the nodes in the circular nominal contact region were moved in the z direction to hit the triangulated surfaces. If a node was in the contact region, it would not hit any triangulated surface, while it would hit two triangulated surfaces if it was in the non-contact region. The z coordinate of the upper hit point was named z_{ij}^m and that of the lower hit point was named z_{ij}^n. Thus, the gap was defined as $g_{ij} = z_{ij}^m - z_{ij}^n$ in non-contact regions and $g_{ij} = 0$ in contact regions. The number of the array elements when $g_{ij} = 0$ was named N_c; this corresponds to the node count in contact regions. The number of the nodes that were in the nominal contact region was named N_n. Thus, the normalized real contact area was $a = N_c/N_n$.

Table 1
Sample details.

Experiment number	Sample	Material	Type of surface	Processing method	Roughness μm
1	1–1	Al	Flat	Turning	3
	1–2	Al	Rough, anisotropic	Milling	60
2	2–1	Al	Flat	Turning	3
	2–2	Al	Rough, anisotropic	Knurling	43
3	3–1	PC	Flat	Turning	3
	3–2	PC	Rough, anisotropic	Milling	60
4	4–1	Al	Rough, isotropic	WEDM	20
	4–2	Al	Rough, isotropic	WEDM	22
5	5–1	PC	Flat	Turning	3
	5–2	PC	Rough, anisotropic	Milling	106
6	6–1	Al	Flat	Turning	3
	6–2	Al	Rough, anisotropic	Milling	56

3.2. Determination of the grid spacing

The spacing d between nodes on the grid can contribute to error in the data processing procedure. If the grid is too coarse (d is very large), some rough surface details will be missed. Theoretically, the finer the grid, the fewer details will be missed such that the data processing procedure will be more accurate. However, a grid with very small spacing can be computationally intensive. Thus, it is important to identify the optimal grid to achieve the lowest data processing error and lowest demand on computing resources. The spacing of the grid is influenced by the spatial resolution of the experiment and the statistical parameters of the rough surfaces. Thus, grid refinement studies should be done to identify the optimal grids. Herein, a series of grids with increasing d were used to process all the experimental data, and the average gap and normalized real contact area calculated from these grids. All experiment surfaces showed a convergence of the contact results as the decreasing of the spacing, experiment 2 with a 5-N squeeze

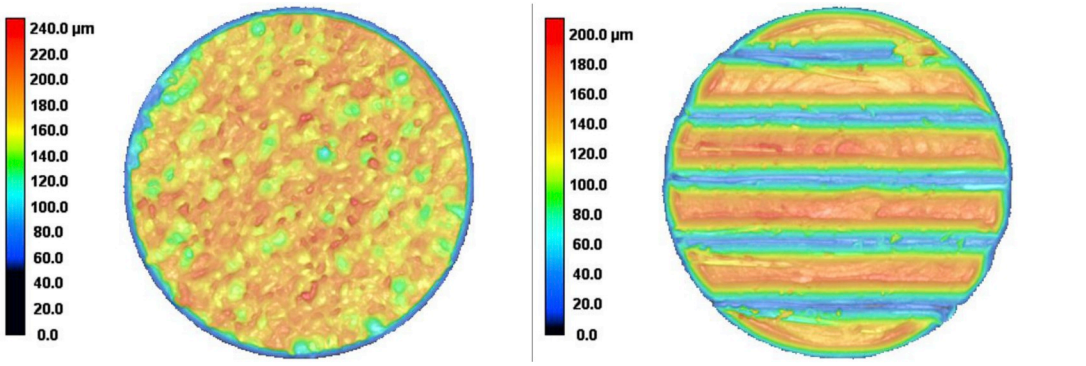

(a) Isotropic rough surface (Sample 4-2). (b) Anisotropic rough surface (Sample 2-2).

Fig. 4. Surface topography (measured using a surface profilometer).

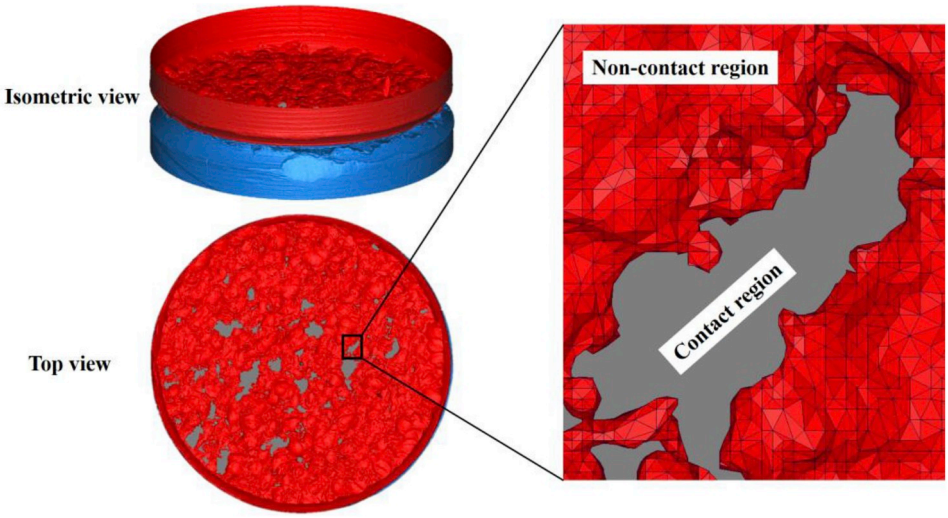

Fig. 5. Geometric model of Experiment 4 with a 100-N load measured using the CT system (grey zones correspond to the contact zone).

load is presented as an example in Fig. 7. As the spacing d decreased from 0.04 to 0.005 mm, the average surface separation and real contact area fluctuated, but remained unchanged when the spacing d further decreased from 0.005 to 0.002 mm. This indicated that 0.005 mm was the largest grid spacing that was not likely to lead to significant data processing error. To ensure the accuracy of the results, all of the experimental data were processed with a 0.002 mm grid spacing.

3.3. Error estimation

Fig. 8 shows that the measured gap g_{ij} has an associated error Δg_{ij} in the vertical direction. This error results from the spatial resolution of the experiment. The error in the real contact area A is between $A^{\min}$ (the lower limit) and $A^{\max}$ (the upper limit).

As noted above, the measured gap is defined as $g_{ij} = z_{ij}^m - z_{ij}^n$, so the gap error is $\Delta g_{ij} \le \Delta z_{ij}^m + \Delta z_{ij}^n$. In Fig. 9, Δz_{ij}^m and Δz_{ij}^n are the errors in height of the measured external surfaces (in the vertical direction). The experimental spatial resolution achieved in this work was 2 μm, such that the identified external surfaces had a maximum error of approximately 2 μm (denoted Δd) perpendicular to the surfaces. The relationship between Δz_{ij}^m and e can be expressed approximately by Equation (1):

$$\Delta z_{ij}^m = \sqrt{(\Delta d)^2 + (\Delta d \cdot \tan\alpha)^2} = \Delta d\sqrt{1 + (\nabla z_{ij}^m)^2} \tag{1}$$

where $\tan\alpha$ is the gradient of the surface at point (x_i, y_j, z_{ij}^m) ($\tan\alpha = \nabla z_{ij}^m$). Likewise, the error in height at point (x_i, y_j, z_{ij}^n) can be calculated based on ∇z_{ij}^n and Δd. The derivation of the gap error Δg_{ij} is shown in Equation (2):

$$\Delta g_{ij} = \sqrt{(\Delta z_{ij}^m)^2 + (\Delta z_{ij}^n)^2} = \Delta d\sqrt{2 + (\nabla z_{ij}^m)^2 + (\nabla z_{ij}^n)^2} \tag{2}$$

Fig. 8 also illuminates that the error in area of true contact can be expressed as $\Delta A = A^{\max} - A^{\min} \approx 2\cdot(A^{\max} - A)$. Thus, the normalized real contact area error (denoted as Δa) can be deduced by Equation (3):

$$\Delta a \approx 2\cdot(a^{\max} - a) \tag{3}$$

where $a^{\max}$ represents the upper limit of the normalized real contact area which is dependent on the lower limit of the gap ($g_{ij} - \frac{1}{2}\Delta g_{ij}$). The number of array elements for which $g_{ij} - \frac{1}{2}\Delta g_{ij} \le 0$ was named $N_c^{\max}$; this corresponds to the maximum possible node count in contact regions. Thus, the upper limit of the normalized real contact area is $a^{\max} = N_c^{\max}/N_n$.

4. Results and discussion

4.1. Evolution and error of the surface separation

The 3D surface separation distribution was obtained by processing the data in the geometric model, and the average gap was calculated based on the 3D surface separation distribution. Fig. 10 presents the

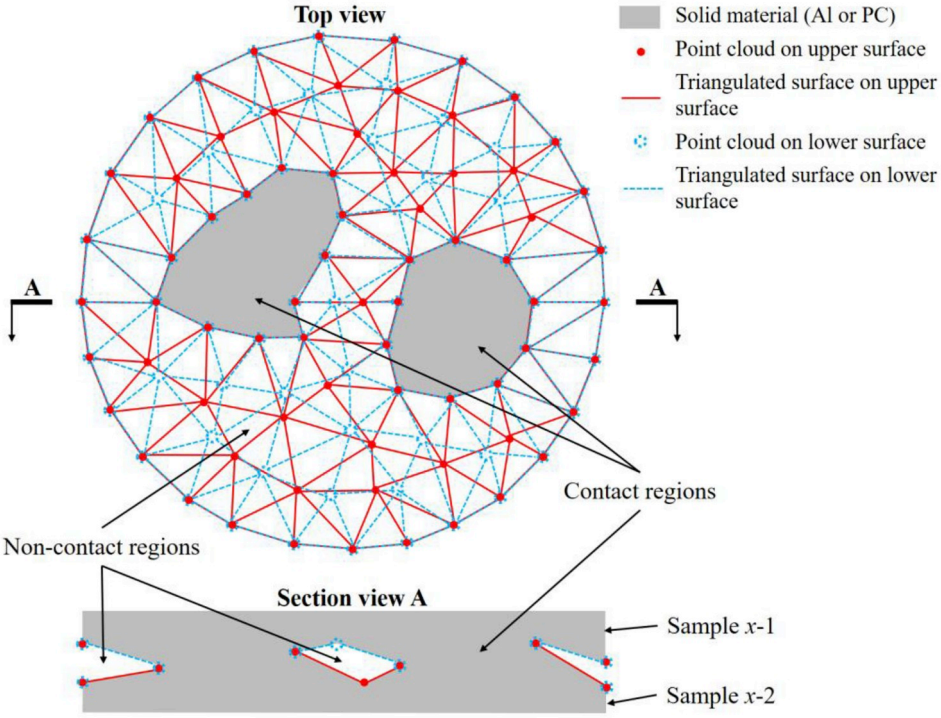

Fig. 6. Sketch of the stereolithography model of an experimentally observed contact pair.

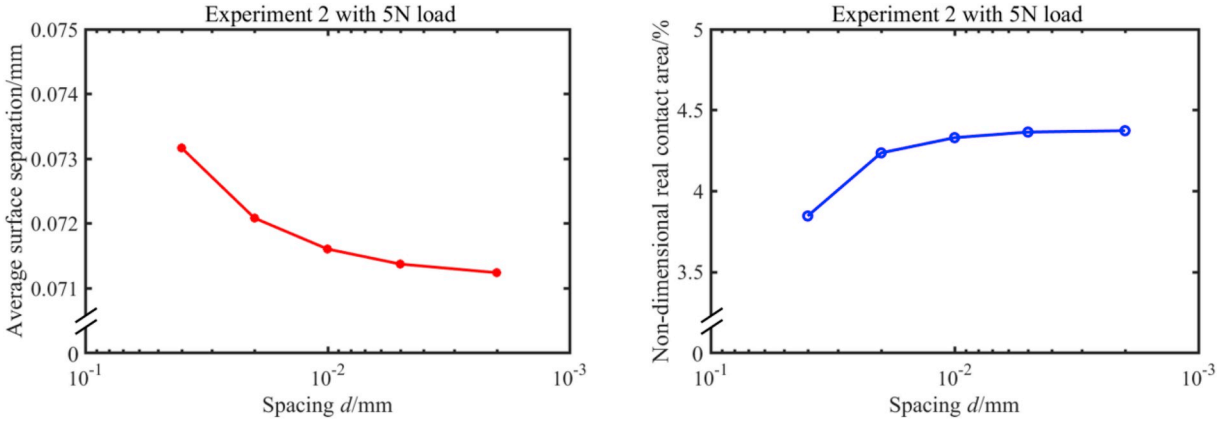

(a) Average surface separation. (b) Normalized real contact area.

Fig. 7. Grid refinement results (Experiment 2 with a 5-N squeeze load is presented as an example).

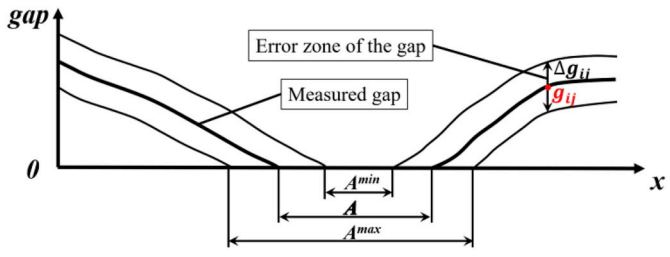

Fig. 8. Measured gap, real contact area, and error (schematic).

evolution of the average gaps and gap errors. The measured errors could be neglected because they were sufficiently small compared with the average gaps. This demonstrated that the evolution of the surface deformation could be measured directly and accurately.

4.2. Evolution and error of the normalized real contact area

The normalized real contact area was calculated by further processing the gap distribution. The evolution of the normalized real contact area over the squeeze pressure are shown in Fig. 11. The errors (Fig. 11) were all relatively small. However, although the error for the isotropic rough surfaces (Experiment 4) clearly decreased with increasing squeeze pressure and real contact area, the errors for the anisotropic surfaces (Experiments 1–3) remained constant. This was attributed to differences in surface topography. For anisotropic surfaces with parallel textures, the perimeter of the contact patches remains constant with increasing real contact area. However, for random rough surfaces, the perimeter lengthens with increasing real contact area.

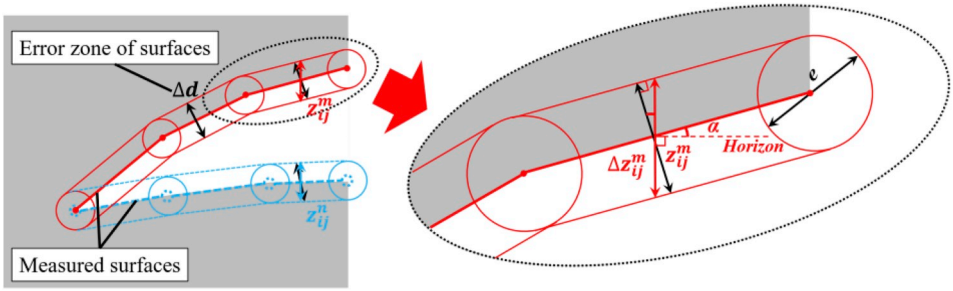

Fig. 9. Measured external surfaces and possible contact zone of the surfaces (schematic).

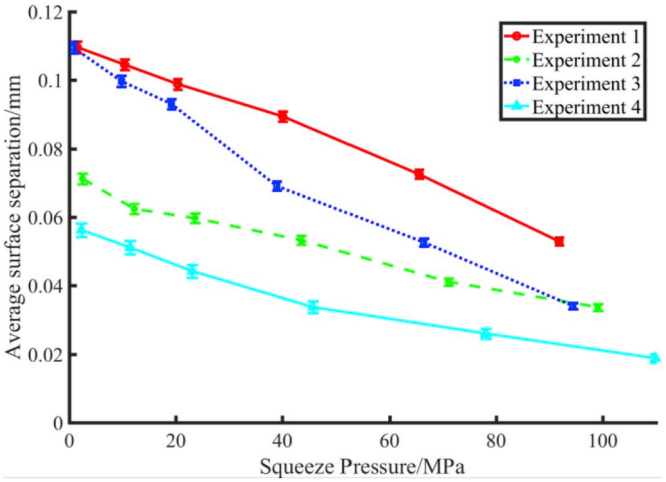

Fig. 10. Evolution of the average surface separation and the errors.

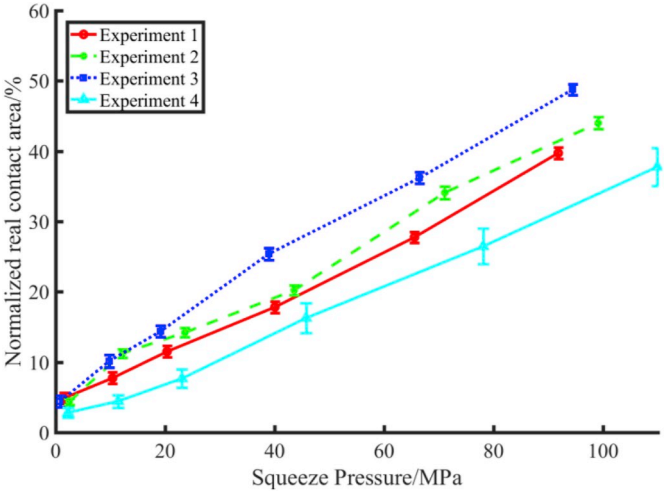

Fig. 11. Evolution of the normalized real contact area and the errors.

4.3. Limitations of our method

The major limitation of this experimental method is the measurement spatial resolution. In our experiments, the spatial resolution was 2 μm, so any zone where the separation was less than 2 μm could be considered as a contact zone. Thus, the measured area of true contact was larger than the actual value. This could explain the nonzero normalized real contact area experimentally measured under conditions of very low load (Fig. 11). Such error would likely be lower for measurements obtained at higher resolution. To ensure the accuracy of the measurements using our material and setup, the roughness of the experimental surfaces should exceed Ra 20 μm. Nano-CT is a rapidly developing technology. The spatial resolution of commercial X-ray CT systems has increased from 2 μm in 2009 to 200 nm currently, and it is predicted to improve further in the future (Table 2). The measurement error of this experimental method will decrease as nano-CT technology further develops.

Another limitation of this method is that the surface topography in the contact regions between two samples made of the same material cannot be identified and measured. However, if the samples are made from different materials, especially materials of different density, this limitation disappears. This is because X-ray CT technology uses density contrast to identify the boundary of the analyte. If the material of two samples is the same, the material density on both sides of the boundary in the contact regions is the same such that the boundary cannot be identified.

4.4. Advantages of our method

The major advantages of this method are that it allows accurate measurement of the 3D gap distribution and area of true contact on assembled rough surfaces that are not transparent.

Compared with current technologies, our CT method also has another important advantage. At present, analytical, numerical, and experimental methods can only solve the contact problem for surfaces that can be represented by an analytical function of two in-plane coordinates (each x, y position has a unique z value); this kind of surface is called an "ideal rough surface" (Fig. 12a). However, the CT experiments revealed more complex contact phenomena because some contact pairs' rough surfaces were not ideal. Fig. 12b shows that some x, y positions of the rough surfaces had more than one z value; these were defined as surface defects. Such surface defects differ from standard surface roughness and cannot be measured using normal optical surface profilometry, nor by other approaches. These defects may significantly influence contact mechanics that cannot be elucidated by current analytical, numerical, and experimental methods.

However, the X-ray CT method can help to solve this problem. Fig. 13 shows the contact behavior of a defective rough surface. The defects might be caused by some unavoidable and unpredictable factors, such as cavities in the material, cracks resulting from the processing stress, and impurities on the surfaces. Furthermore, Fig. 14 shows how ideal rough

Table 2
Spatial resolution of commercial X-ray computed tomography systems.

Date	Product	Maximum resolution (μm)	Maximum resolution under experimental conditions (μm)
2009	phoenix v|tome|x s	2	–
2011	phoenix nanotom s	0.5	4
Current	phoenix nanotom s	0.2	2

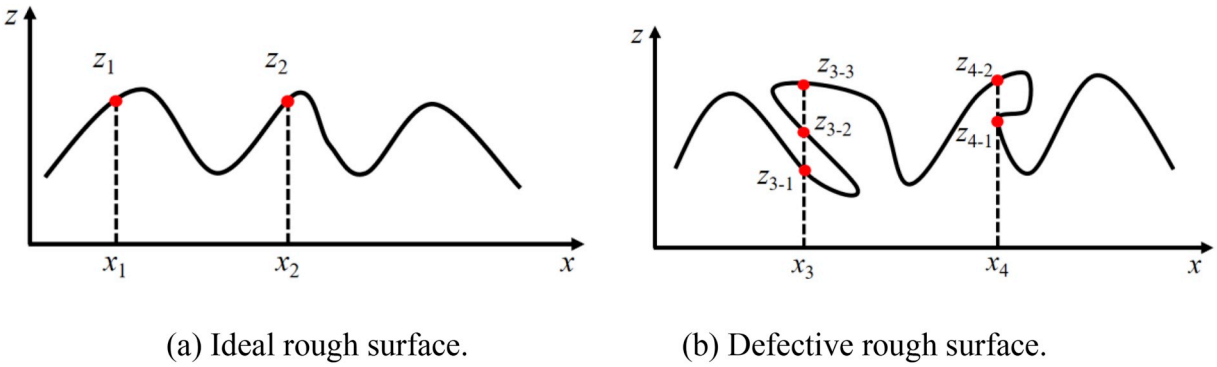

Fig. 12. Sketches of ideal and defective rough surfaces.

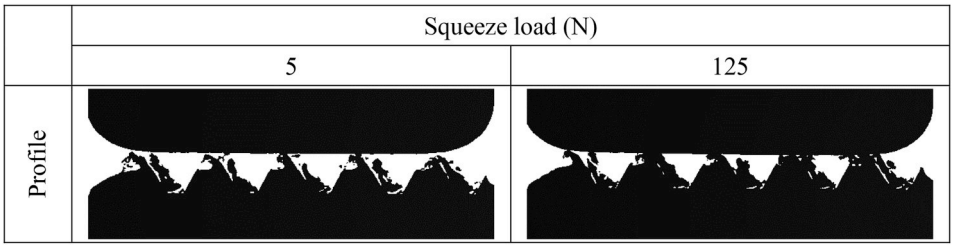

Fig. 13. Contact behavior with surface defects (Sample 5–2).

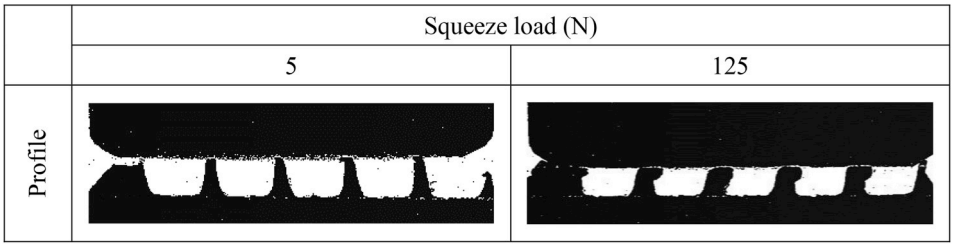

Fig. 14. Contact behavior involving shearing of asperities (Sample 6–2).

surfaces can become defective due to shearing of asperities caused by tangential deformation. These contact phenomena cannot be observed by conventional approaches, but can be investigated using the X-ray CT method.

5. Conclusions

It is difficult to accurately measure the area of true contact and gap distribution on assembled rough interfaces, particularly on non-transparent surfaces. In this study, the capability of the novel experimental method based on X-ray CT technology used in Ref. [1] to study the contact mechanics on assembled non-transparent rough interfaces was further investigated. To facilitate the reproduction of this work by other researchers, the experimental procedure and data-processing method are described in detail. The evolution of the surface deformation and the normalized real contact area over the squeeze pressure were investigated using this method, and the experimental error was also estimated. Furthermore, complex contact behaviors involving surface defects and the shearing of asperities were also observed; such behaviors cannot be investigated using other current methods. This is yet another advantage of the CT technology.

The spatial resolution is the main limitation of this technology. We achieved a resolution of 2 μm, which is sufficient to demonstrate that current X-ray CT technology is capable of analyzing contact between rough surfaces at the micron scale. It remains challenging to study contact mechanics at smaller scales, although use of an advanced CT system (with a higher-power X-ray source or a higher-resolution detector) might improve the spatial resolution and enable analysis of a larger sample. Another limitation of this experimental method is that CT technology cannot identify the boundaries between rough surfaces in the contact region if the contact surfaces are of the same density.

Funding

This work was supported by the National Natural Science Foundation of China (Grant No. 51975055 and 51935003), the Equipment Pre-Research Foundation of China (Grant No. JZX7Y20190250027501), and the International Graduate Exchange Program of Beijing Institute of Technology, China.

Author contribution section

Feikai Zhang: Methodology, Software, Formal analysis, Investigation, Writing - Original Draft, Visualization.

Jianhua Liu: Resources, Supervision, Project administration, Funding acquisition.

Xiaoyu Ding: Conceptualization, Methodology, Writing - Review & Editing, Funding acquisition.

Zhimeng Yang: Validation, Data Curation, Visualization.

Declaration of competing interest

The authors declare that they have no known competing financial interests or personal relationships that could have appeared to influence the work reported in this paper.

Acknowledgements

Professor J. R. Barber of University of Michigan provided several constructive suggestions and comments to this work. Here, the authors would like to show their sincere appreciation to him.

Appendix A. Experimental measured probability distribution of gap for the random rough surface

Notably, the probability distribution of gap for the random rough surface has also been calculated (as shown in Fig. A), as it is decisive for the leak rate of Reynolds flow through leak channels. When the squeeze load is small, there is only one peak on the distribution curve. With the increase of the squeeze load, a second peak with very small gap exists. The detailed discussion on this phenomenon can be found in Ref. [33].

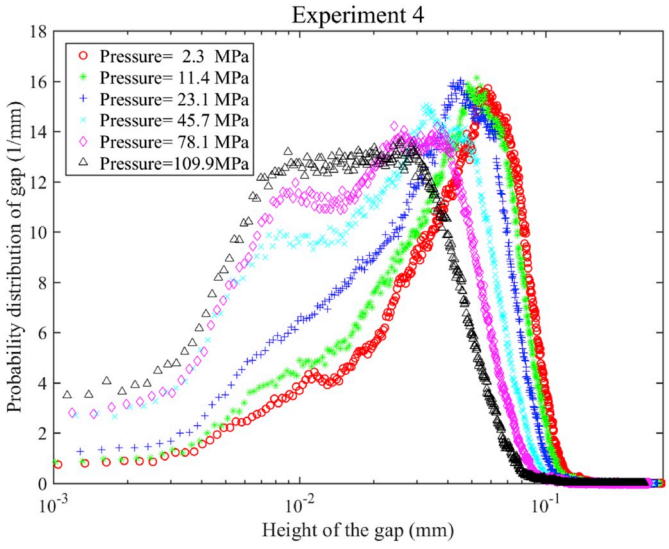

Fig. A. Probability distribution of gap for the random rough surface (Experiment 4).

Appendix B. Experimental measured contact pressure, average surface separation, and real contact area (Table A, B, C and D)

Table A
Experiment 1

Contact pressure (MPa)	1.5	10.4	20.4	40.1	65.6	91.8
Average gap (μm)	109.6	104.5	98.9	89.4	72.5	52.9
Real contact area (%)	4.9	7.7	11.5	17.8	27.8	39.7

Table B
Experiment 2

Contact pressure (MPa)	2.5	12.2	23.6	43.6	71.1	99.1
Average gap (μm)	71.2	62.4	59.7	53.3	41.1	33.7
Real contact area (%)	4.4	11.3	14.2	20.2	34.1	44.0

Table C
Experiment 3

Contact pressure (MPa)	0.8	9.8	19.2	39.0	66.5	94.5
Average gap (μm)	109.5	99.7	93.0	69.1	52.6	34.0
Real contact area (%)	4.4	10.2	14.4	25.4	36.2	48.8

Table D
Experiment 4

Contact pressure (MPa)	2.3	11.4	23.1	45.7	78.1	109.9
Average gap (μm)	56.3	51.1	44.3	33.7	26.0	18.8
Real contact area (%)	2.8	4.4	7.7	16.3	26.5	37.8

References

[1] Zhang F, Liu J, et al. Experimental and finite element analyses of contact behaviors between non-transparent rough surfaces. J Mech Phys Solids 2019;126:87–100.
[2] Dapp WB, Andreas L, et al. Self-affine elastic contacts: percolation and leakage. Phys Rev Lett 2012;108:244301.
[3] Lorenz B, Persson BNJ. Leak rate of seals: comparison of theory with experiment. Epl 2009;86:44006.
[4] Vakis AI, Yastrebov VA, et al. Modeling and simulation in tribology across scales: an overview. Tribol Int 2018.
[5] Woo KL, Thomas TR. Contact of rough surfaces: a review of experimental work. Wear 1980;58:331–40.
[6] Xu Y, Chen Y, et al. A new method for the measurement of real area of contact by the adhesive transfer of thin Au film. Tribol Lett 2018;66:32.
[7] Boeschoten F, Held EFMVD. The thermal conductance of contacts between aluminium and other metals. Physica 1957;23:37–44.
[8] Bhushan B. The real area of contact in polymeric magnetic media-II: experimental data and analysis. Tribol Trans 1985;28:181–97.
[9] Nagy PB. Ultrasonic classification of imperfect surfaces. J Nondestruct Eval 1992;11:127–39.
[10] Dwyer-Joyce RS, Drinkwater BW, et al. The use of ultrasound in the investigation of rough surface interfaces. J Tribol 2001;123:8–16.
[11] Selvadurai P, Glaser S. Direct measurement of contact area and seismic stress along a sliding interface. In: 46th US rock mechanics/geomechanics symposium. American Rock Mechanics Association; 2012.
[12] Lekue J, Dörner F, et al. On the source of the systematic error of the pressure measurement film applied to wheel–rail normal contact measurements. J Tribol 2018;140:024501.
[13] Nitta I, Matsuzaki Y. Experimental study of the performance of static seals based on measurements of real contact area using thin polycarbonate films. J Tribol 2010;132:022202.
[14] Visscher M, Hendriks CP, et al. The real area of contact measured on elastomers. Thin Films in Tribology 1993;19:705–14.
[15] Visscher M, Struik KG. Optical profilometry and its application to mechanically inaccessible surfaces part I: principles of focus error detection. Precis Eng 1994;16:192–8.
[16] Visscher M, Hendriks CP, et al. Optical profilometry and its application to mechanically inaccessible surfaces part II: application to elastometer/glass contacts. Precis Eng 1994;16:199–204.
[17] Hendriks CP, Visscher M. Accurate real area of contact measurements on polyurethane. J Tribol 1995;117:607–11.
[18] Dieterich JH, Kilgore BD. Direct observation of frictional contacts: new insights for state-dependent properties. Pure Appl Geophys 1994;143:283–302.
[19] Dieterich JH, Kilgore BD. Imaging surface contacts: power law contact distributions and contact stresses in quartz, calcite, glass and acrylic plastic. Tectonophysics 1996;256:219–39.
[20] Benabdallah SM, Lapierre J. A new device for measuring the real area of contact of polymeric material by the perturbation of total internal reflection. J Mater Sci 1990;25:3497–500.
[21] Bennett AI, Harris KL, et al. Contact measurements of randomly rough surfaces. Tribol Lett 2017;65:134.
[22] Rohde SE, Bennett AI, et al. Measuring contact mechanics deformations using DIC through a transparent medium. Exp Mech 2017;57:1445–55.
[23] Bennett AI, Rohde S, et al. Deformation measurements of randomly rough surfaces. Tribol Lett.65:123.
[24] Berthe L, Sainsot P, et al. Plastic deformation of rough rolling contact: an experimental and numerical investigation. Wear 2014;312:51–7.
[25] Yusof NFM, Ripin ZM. A technique to measure surface asperities plastic deformation and wear in rolling contact. Wear 2016;368:496–504.
[26] Kriston A, Fülöp T, et al. A novel method for contact analysis of rubber and various surfaces using micro-computerized-tomography. Polym Test 2016;53:132–42.
[27] Roussos C, Swingler J. The 3D nature of a real un-dismantled electrical contact interface. Wear 2015;328:115–22.
[28] Roussos CC, Swingler J. A 3D contact analysis approach for the visualization of the electrical contact asperities. AIP Adv 2017;7:015023.
[29] Zbrowski A, Matecki K. The use of computed tomography to analyse grinding smudges and subsurface defects in roller bearing rings. Strojniski Vestnik - Journal of Mechanical Engineering 2014;60:709–15.
[30] Yoshinaka F, Nakamura T, et al. Non-destructive observation of internal fatigue crack growth in Ti–6Al–4V by using synchrotron radiation μCT imaging. Int J Fatigue 2016;93:397–405.
[31] Sakdinawat A, Attwood D. Nanoscale x-ray imaging. Nat Photonics 2009;4:840–8.
[32] Goldman LW. Principles of CT and CT technology. J Nucl Med Technol 2007;35:115–28.
[33] Müser MH, Dapp WB, et al. Meeting the contact-mechanics challenge. Tribol Lett 2017;65:118.